Journal of Magnetism and Magnetic Materials 505 (2020) 166758

Contents lists available at ScienceDirect

Journal of Magnetism and Magnetic Materials

journal homepage: www.elsevier.com/locate/jmmm

Research articles

Voltage-controlled magnetic anisotropy in antiferromagnetic $L1_0$-MnPt and MnPd thin films

Yurong Su[a], Mengyin Li[b], Jia Zhang[b,*], Jeongmin Hong[a], Long You[a,*]

[a] School of Optical and Electronic Information, Huazhong University of Science and Technology, 430074 Wuhan, China
[b] School of Physics and Wuhan National High Magnetic Field Center, Huazhong University of Science and Technology, 430074 Wuhan, China

ABSTRACT

The efficient electrical control of the magnetic states of antiferromagnets is one of the main focus in antiferromagnetic spintronics. In this work, the voltage-controlled magnetic anisotropy (VCMA) effect in two representative antiferromagnets $L1_0$-type MnPt and MnPd thin films has been investigated by employing first-principles calculations. Our results indicate that both of the MnPt and MnPd films show in-plane magnetic anisotropy and the magnetic easy axis points either along [1 0 0] or [1 1 0] direction depending on the film thickness. The applied electric field in the range of −0.3 V/Å and + 0.3 V/Å (vacuum as dielectric) leads to the change of magnetocrystalline anisotropy of both films at the order of tens of μJ/m^2. Especially, for MnPt film with thickness of two unit cells on Pt(0 0 1), it shows that the moderate electric field is able to switch the in-plane magnetic easy axis between [1 0 0] and [1 1 0] directions. For MnPd thin films, the VCMA effect shows generally linear dependence on the electric field and the VCMA coefficients are estimated in the range of 2.7 to 22.6 fJ/V/m. Our calculation results may stimulate future investigations on the VCMA effect of metallic antiferromagnetic films and pave the possible applications in memory device.

Recently, antiferromagnets (AFMs) have attracted increasing research interest due to their advantages superior to ferromagnets (FMs) [1–3]. For instance, AFMs are robust against magnetic field perturbation and has null stray fields. Furthermore, compared to FMs, AFMs display ultrafast spin dynamics due to the high magnetic resonance frequency, which in principle, allows the antiferromagnetic devices work at THz dynamic speeds [4,5]. These features enable AFMs especially appealing for applications in high-density memory devices [6,7]. However, how to effectively manipulate the magnetization states by electrical means is one of the main challenge for the practical applications of AFMs.

Various approaches have been proposed including magnetic, strain, electrical, and optical ways to manipulate magnetic states of AFMs [8]. Among them, one promising approach is to use current-induced spin-orbit torques, which have been extensively used for electrical writing in FM-based magnetic random access memories (MRAMs) [9–11]. Recently spin-orbit torques have also been successfully demonstrated for control of the AFM moments [12]. Nevertheless, at present the AFM materials which are suitable for electric current manipulation are limited to special materials with staggered spin accumulation, such as CuMnAs and Mn_2Au. Besides, typically the electric current density required for the rotation of the Néel vector in those materials is at the order of 10^6 and 10^7 A/cm^2, which should be further decreased for low power consumption devices [7,13–15].

The control of the Néel order in AFMs via voltage or electric field may be more favorable towards energy efficient spintronic devices. At present, the electric field control of AFM has been mainly focused on the strain effect. For example, recent experiments demonstrate that the Néel vector in MnPt and Mn_2Au can be rotated at room temperature by electric field induced strain arising from piezoelectric substrate [16,17]. However, the manipulation of magnetic anisotropy of AFMs by using the pure electric field or voltage effect may be more straightforward for practical applications. The voltage-controlled magnetic anisotropy (VCMA) in FMs, for example in Fe/MgO interface, have been extensively investigated both from experiments and theories. This effect has been thought as one of the promising strategies for the next-generation VC-MRAM (voltage controlled MRAM) due to the ultralow power consumption and ultrafast time scale (< sub-nanosecond) [18–22]. However, the VCMA effect in AFMs has been rarely studied. In this letter, the VCMA effect in two representative metallic AFMs, $L1_0$-type MnPt and MnPd thin films are investigated by using first-principles calculations.

The atomic structures of bulk MnPt and MnPd are shown in Fig. 1(a). In the past, MnPt, MnPd and the same class of Mn-based $L1_0$-type AFMs have been used as the pinning layer in spin-valve-like GMR and TMR devices [1,23,24]. The metallic AFMs MnPt and MnPd have relative high Néel temperature, which make them suitable for practical applications. For example, for MnPt the Néel temperature T_N is 970 K and for MnPd T_N is 810 K. Recent first-principles calculations also indicate that the Néel vector of both materials can be rotated by changing

* Corresponding authors.
E-mail addresses: jiazhang@hust.edu.cn (J. Zhang), lyou@hust.edu.cn (L. You).

https://doi.org/10.1016/j.jmmm.2020.166758
Received 29 December 2019; Received in revised form 14 March 2020; Accepted 16 March 2020
Available online 17 March 2020
0304-8853/

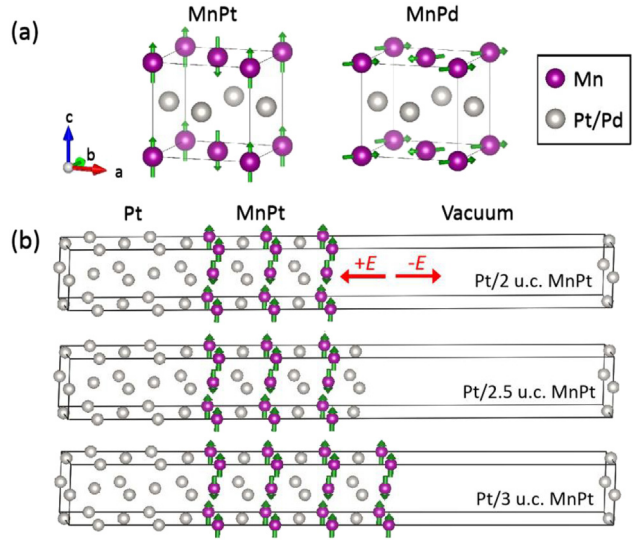

Fig. 1. The illustrations of atomic structures of bulk $L1_0$-type MnX (X = Pt, Pd) and the corresponding film structures. (a) Atomic and calculated ground magnetic structures of bulk $L1_0$ MnPt and MnPd. The magnetization axis is along [0 0 1] in bulk MnPt and along [1 1 0] in bulk MnPd. (b) The side view of the Pt/MnPt/Vacuum structure with 2 u.c., 2.5 u.c. and 3 u.c. of MnPt. The red arrows indicate the definition of positive and negative electric fields. The Green arrows show the magnetic moment direction on Mn atoms. (For interpretation of the references to colour in this figure legend, the reader is referred to the web version of this article.)

the magnetocrystalline anisotropy (MCA) via the variation of lattice constant through strain effect [25]. In addition, earlier theoretical calculations indicate that the MCA of bulk $L1_0$-MnPt is sensitive to the number of electron [26]. Those properties make MnPt and MnPd films suitable for the investigations of the VCMA effect.

The atomic structures of Pt/MnX (X = Pt, Pd)/Vacuum with different thickness of MnX films are shown in Fig. 1b. The five monolayers (MLs) of fcc Pt (0 0 1) serves as substrate and the thickness of vacuum is larger than 15 Å in order to minimize the artificial interactions between asymmetric surface layers in a supercell. The electric field is applied across the whole structure by introducing a dipole layer placing in the vacuum region [27]. The direction of the applied electric field is shown in Fig. 1(b), where positive electric field is pointing towards of MnX surface and negative electric field is pointing outwards of MnX surface.

The first-principles calculations are performed by using the Vienna *ab initio* simulation package (VASP) code [28] implemented with the projector-augmented-wave (PAW) method [29], within the Perdew-Burke Ernzerhof (PBE) type of generalized gradient approximation (GGA) for the exchange correlation potential [30]. A plane-wave cutoff energy is 400 eV. The in-plane lattice constants are fixed to that of the corresponding bulk values (a = b = 3.98 Å for MnPt and a = 3.99 Å for MnPd), while the atomic positions of the whole films have been fully relaxed in the absence of electric field until the ionic Hellmann-Feynman forces on each atom are less than 1 meV/Å. The calculated lattice constants and the magnetic moments on the Mn sites in bulk MnPt and MnPd agree with previous theoretical results by using the PBE-GGA [25,31,32]. After ion relaxation, the resulting atomic structures are then used to calculate the VCMA effect by applying various electric fields across the film. The electron density for thin films are self-consistently calculated by using a 24 × 24 × 1 k-point mesh. For the calculations of MCA, a much denser k-point mesh 35 × 35 × 1 is used which is necessary to converge the MCA at the order of 5 μeV per unit cell. The MCA is determined by the so-called standard force theorem [19,20,33,34]. First, a self-consistent calculation is performed in the absence of spin–orbit coupling (SOC) in order to obtain the converged electron density. Then, one step of calculation in the presence of SOC

Table 1
The calculated $MCA_{[1\ 0\ 0]}$ (E_{band}[1 0 0]-E_{band}[0 0 1]) and $MCA_{[1\ 1\ 0]}$ (E_{band} [1 1 0]-E_{band}[0 0 1]) (in the unit of mJ/m^2) in Pt/MnX (X = Pt, Pd) thin films in the absence of electric field. The MCAs in bulk MnPt and MnPd (in the unit of meV/u.c.) are also listed for comparison.

System	$MCA_{[1\ 0\ 0]}$	$MCA_{[1\ 1\ 0]}$	$MCA_{[1\ 1\ 0]}$-$MCA_{[1\ 0\ 0]}$	Easy axis
5 ML Pt/1 u.c. MnPt	−3.095	−3.145	−0.050	[1 1 0]
5 ML Pt/2 u.c. MnPt	−1.034	−0.977	0.057	[1 0 0]
5 ML Pt/2.5 u.c. MnPt	−2.863	−2.543	0.320	[1 0 0]
5 ML Pt/3 u.c. MnPt	−0.851	−0.709	0.142	[1 0 0]
5 ML Pt/1 u.c. MnPd	−1.077	−1.122	−0.045	[1 1 0]
5 ML Pt/2 u.c. MnPd	−0.130	−0.027	0.103	[1 0 0]
5 ML Pt/2.5 u.c. MnPd	−1.385	−1.437	−0.052	[1 1 0]
5 ML Pt/3 u.c. MnPd	−0.819	−0.804	0.015	[1 0 0]
Bulk MnPt[a)]	0.174	0.176	0.002	[0 0 1]
Bulk MnPd[b)]	−0.565	−0.576	−0.011	[1 1 0]

[a)-b)]The unit of MCA in bulk MnPt and MnPd is in meV/u.c.

with the Néel vector pointing along different directions is performed. The MCA is defined as the band energy difference for the magnetization along the arbitrary direction [abc] and perpendicular [0 0 1] direction: MCA = E_{band}[abc] − E_{band}[0 0 1].

According to our calculation results shown in Table 1, the magnetic moment of Mn atoms in bulk MnPt is along [0 0 1] direction and in bulk MnPd is along [1 1 0] direction lying on the *ab*-plane, which agrees with previous experimental findings [35,36]. The MCA values for bulk MnPt and MnPd are also consistent with the earlier calculated results [25]. In comparison, the magnetic ground states of MnPt and MnPd thin films are different from the corresponding bulk cases. The MCAs in MnPt and MnPd films with different thickness on Pt (0 0 1) under zero electric field are listed in Tabel I. The easy axis of 1 u.c. MnPt film on Pt (0 0 1) is found to be along [1 1 0] direction, in other cases it is along [1 0 0] direction. However, MnPd always show in-plane easy axis both in bulk and thin film cases. The MCA of MnPd film oscillates with increasing film thickness and the easy axis can either be [1 0 0] or [1 1 0]. In general, for both AFM films the MCA energy difference between in-plane [1 0 0] and [1 1 0] directions are small, indicating that the rotation of the Néel vector in the film plane by pure VCMA effect may be possible.

In the thin film geometry, the electric field is applied by employing the dipole moment method [27]. Fig. 2 shows the planar-averaged electrostatic potential across the supercell. The change of electrostatic potential distribution under various electric fields is consistent with the expectation, that is the potential energy is linear with the distance in vacuum region and keeps constant inside of the metallic films. This confirms the desired electric fields have been correctly applied across the films.

Fig. 3 depicts the calculated MCA as a function of electric field on MnPt and MnPd films with thickness of 2, 2.5 and 3 u.c. The blue and red lines represent the $MCA_{[1\ 0\ 0]}$ ($MCA_{[1\ 0\ 0]}$ = E_{band}[1 0 0]-E_{band} [0 0 1]) and $MCA_{[1\ 1\ 0]}$ ($MCA_{[1\ 1\ 0]}$ = E_{band}[1 1 0]-E_{band}[0 0 1]), respectively. It shows that the magnetic moments of Mn always lie in the *ab*-plane under various electric fields. One of the interesting result is that for MnPt with thickness of 2 u.c., at certain electric field range, the easy axis can be switched between in-plane [1 0 0] and [1 1 0] directions. For example, when the electric field is in the range of −0.3 V/Å and −0.15 V/Å, the $MCA_{[1\ 1\ 0]}$ is less than $MCA_{[1\ 0\ 0]}$, which means the Néel vector can be rotated by 45°in the *ab*-plane by applying electric field. In other cases, since the magnetization direction of the thick MnPt layer cannot be rotated by electric field, the Néel vector of MnPt stays at [1 0 0] direction (except for t = 3 u.c. at 0.2 V/Å).

In addition, the modulation of MCA is more notable when the surface is terminated with Mn atoms. For example, as for 2 u.c. and 3 u.c. MnPt films with Mn termination, the two curves represented $MCA_{[1\ 0\ 0]}$

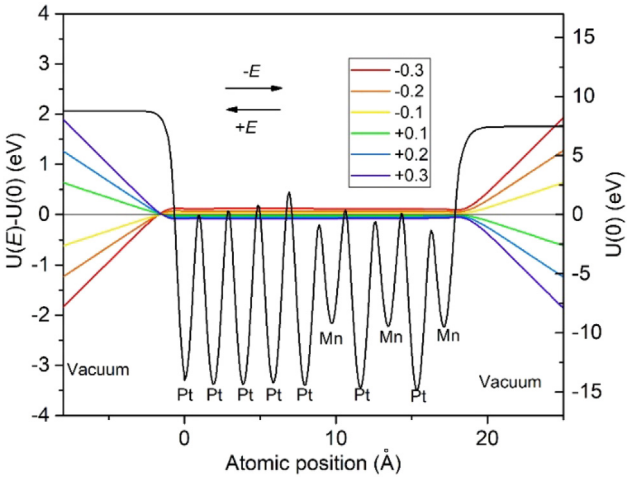

Fig. 2. . The planar-averaged electrostatic potential energy distribution of Pt/MnPt (2 u.c.) at zero electric field (black line) and the change of the electrostatic potential energy (U(*E*)-U(0)) when various electric fields are applied across the film. The arrows indicate the direction of the electric field.

and $MCA_{[1\ 1\ 0]}$ crosses at certain points, but for 2.5 u.c. MnPt film with Pt termination the energy difference between two energy lines is large. Generally, for the case of MnPd films as it is shown in Fig. 3(b), the MCA curves looks more or less linear versus electric field. The VCMA effect of MnPd films, which can be quantified by the so-called VCMA coefficient β ($\Delta MCA = \beta E$) has been calculated and summarized in Table 2. For example, for Pt/MnPd(3 u.c.), the VCMA coefficient β is estimated to be 22.6 fJ/V/m by evaluating from the $MCA_{[1\ 1\ 0]}$ curve as it is shown in Fig. 3b. The value of VCMA coefficient β is around 10 times less than that of ferromagnetic Fe/MgO interface and suggests a smaller VCMA effect in the studied antiferromagnetic film.

For the tetragonal lattice, according to the lattice symmetry, the phenomenological magnetic anisotropy energy can be expanded as follows:

$$E(\theta, \phi) = K_{2\perp}\sin^2\theta + K_{4\perp}\sin^4\theta + K_{4||}\sin^4\theta\cos 4\phi \quad (1)$$

where θ (ϕ) is the angle between the direction of magnetic moment and the *c* (*a*) axis, $K_{2\perp}$ is the uniaxial MCA constant, $K_{4\perp}$and $K_{4||}$ are the corresponding fourth-order out-of-plane and in-plane MCA constants. Since the easy axis of MnPt film stays in the *ab*-plane ($\theta = 90^\circ$), by

Table 2
The VCMA coefficients β for MnPd thin films with different thickness are evaluated by linear fitting from Fig. 3b to extract the slope.

MnPd film thickness	β extracted from $MCA_{[1\ 0\ 0]}$ (fJ/V/m)	β extracted from $MCA_{[1\ 1\ 0]}$ (fJ/V/m)
2 u.c.	16.2	9.5
2.5 u.c.	11.9	2.7
3 u.c.	22.1	22.6

referring to the energy at [1 0 0] direction, the MCA here can be written as $E_{band}(90, \phi)$-$E_{band}[1\ 0\ 0] = K_{4||}\cos 4\phi$. For $K_{4||} < 0$, the easy axis is along [1 0 0] direction ($\phi = 0$), and for $K_{4||}$greater than 0, the [1 1 0] axis ($\phi = 45^\circ$) becomes the easy axis. Fig. 4(a) shows the in-plane MCA curves under various electric fields for MnPt with the thickness of 2 u.c. It clearly demonstrates the Néel vector can be switched from [1 0 0] to [1 1 0] by applying appropriate electric fields. The extracted in-plane MCA constants $K_{4||}$ under various electric field are shown in Fig. 4(b). The sign reversal of $K_{4||}$ also indicates the switching of the Néel vector between [1 0 0] and [1 1 0]. In comparison to recent experiments [13–15], where a relative large current density is needed to switch the Néel vector between [1 1 0] and [1 0 0] direction in Mn_2Au, here we demonstrate that in an ultrathin antiferromagnetic MnPt films, the similar manipulation of Néel vector can occur by using pure electric field effect.

In the following, based on the second order perturbation theory, we will try to understand the calculation result especially for Pt(5 MLs)/MnPt (2 u.c.) film. The spin–orbit coupling (SOC) Hamiltonian can be written as:

$$H_{soc} = \xi(r)\vec{\sigma}\cdot\vec{L} \quad (2)$$

where *L* is the orbital angular momentum operator, σ is the Pauli matrix, ξ is the atomic spin–orbit coupling strength. According to the second order perturbation theory, the MCA can be understood from the magnetization axis dependence of spin–orbit coupling energy correction to the total energy.

The spin-conserved energy correction due to the SOC can be written as:

$$E_{soc}(M_\eta) = -\frac{\xi^2}{4}\sum_{o,u}\frac{|\langle\psi_o|\ L_\eta\ |\psi_u\rangle|^2}{\varepsilon_u - \varepsilon_o} \quad (3)$$

where L_η is the orbit angular momentum operator which is dependant

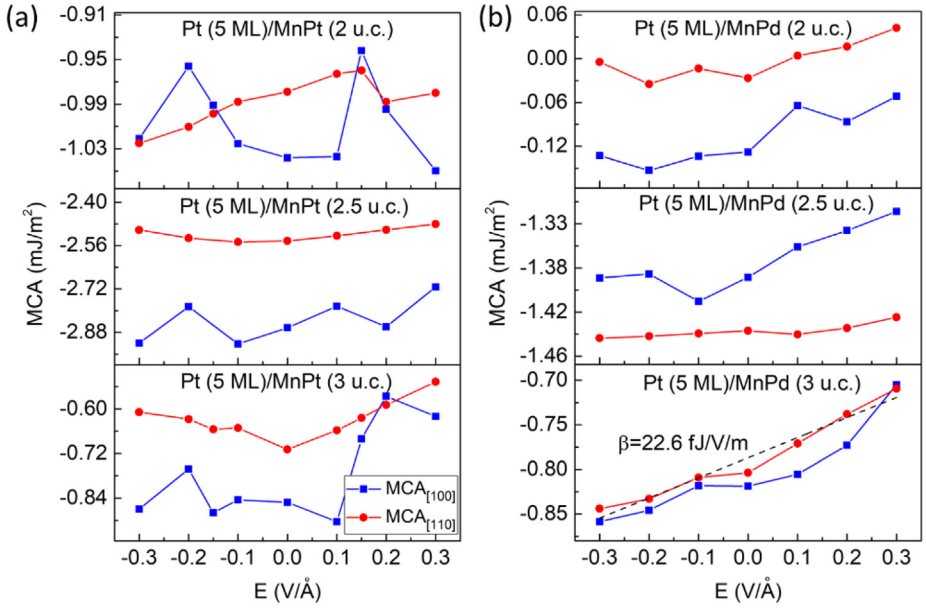

Fig. 3. . The calculated MCA as a function of applied electric field in the range of ± 0.3 V/Å for (a) Pt/MnPt and (b) Pt/MnPd with MnX (X = Pt, Pd) film thicknesses of 2, 2.5 and 3 u.c. The red line shows the $MCA_{[1\ 1\ 0]}$ (E_{band}[1 1 0]-E_{band}[0 0 1]) and the blue line shows $MCA_{[1\ 0\ 0]}$ (E_{band}[1 0 0]-E_{band} [0 0 1]). The dashed line for Pt/MnPd (3 u.c.) in (b) shows the linear fitting of $MCA_{[1\ 1\ 0]}$. (For interpretation of the references to colour in this figure legend, the reader is referred to the web version of this article.)

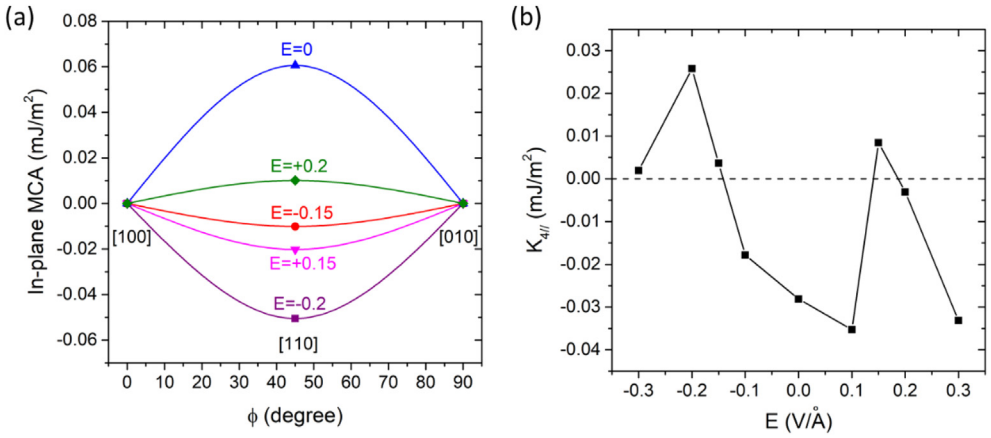

Fig. 4. . (a) The in-plane MCA energy curve ($E_{(\theta=90,\ \phi)} - E_{[1\ 0\ 0]}$) for Pt/MnPt (2 u. c.) under various electric fields. (b) The extracted in-plane MCA constant $K_{4||}$ as a function of the electric field for Pt(5 MLs)/MnPt (2 u.c.).

on magnetization direction η, for instance $L_\eta = L_z$ and L_x when magnetization points along z [0 0 1] and x [1 0 0] directions respectively. Ψ_o and Ψ_u is the occupied (above Fermi energy) and unoccupied (below Fermi energy) wave function without SOC, and ε_o and ε_u are the corresponding eigenvalues. Please note that the second order perturbation of SOC correction to energy E_{soc} is always negative which means SOC will lower down the energy of the system.

The SOC energy difference between different magnetization axis produce the MCA, for instance the energy difference when the magnetization direction is along x and z axis is:

$$E_{MCA} = E_{soc}(M_x) - E_{soc}(M_z) = \frac{\xi^2}{4}\sum_{o,u}\frac{|\langle\psi_o|\ L_z\ |\psi_u\rangle|^2 - |\langle\psi_o|\ L_x\ |\psi_u\rangle|^2}{\varepsilon_u - \varepsilon_o} \tag{4}$$

And further, by integrating over the k space, MCA can be approximately expressed by the production of density of states and the matrix elements of orbital angular momentum operator between different d orbitals as follows:

$$E_{MCA} = \frac{\xi^2}{4}\sum_{\mu,\mu'} P_{\mu\mu'}\int_{-\infty}^{\varepsilon_F} d\varepsilon \int_{\varepsilon_F}^{\infty} d\varepsilon' \frac{\rho_\mu(\varepsilon)\rho_{\mu'}(\varepsilon')}{\varepsilon' - \varepsilon};$$

$$P_{\mu\mu'} = (|\langle d_\mu|\ L_z\ |d_{\mu'}\rangle|^2 - |\langle d_\mu|\ L_x\ |d_{\mu'}\rangle|^2) \tag{5}$$

where d_μ is one of the five d-orbitals d_{xy}, d_{yz}, d_{xz}, $d_{x2\text{-}y2}$ and d_{z2} which is denoted by index μ. $\rho_\mu(\varepsilon)$ is the density of states (DOS) and ε_F is the Fermi energy. The non-vanishing matrix element of L_η between different d-orbitals will contribute to the SOC energy and favor the magnetization along η direction. From the above perturbation analysis, one can find that both of the MCA and VCMA will be closely related to the distribution of DOS around Fermi energy.

According to Eqs. (2)–(5), part of the calculation results can be qualitatively understood from the density of states around Fermi energy. For example, from the density of states shown in Fig. 5(a), one can find for Pt(5 MLs)/MnPt (2 u.c.) film, the main DOS present around Fermi energy have the d_{xy} and d_{yz} orbital features (The DOS of d_{xy} and d_{yz} orbital degenerates due to the four-fold rotation symmetry of the crystal structure). On the other hand, the non-vanishing d orbital matrix element of orbital angular moment for M//x involve the pair of d_{xy} and d_{yz}. For L_x, one of the non-vanishing matrix element is $\langle d_{xy}|\ L_x\ |d_{xz}\rangle = -i$, which indicates the DOS distribution around Fermi energy shown in Fig. 5(a) will contribute to E_{soc} for M//x and favor the inplane easy axis. This is consistent with the calculation result that the [1 0 0] is the magnetization easy axis for Pt(5 MLs)/MnPt (2 u.c.) film.

The electrons at the surface of metallic films will redistribute under the electric field and therefore the density of states around Fermi energy will be modified. In consequence, the MCA will be changed by applying electric field. Fig. 5(b) shows the DOS of Mn atom for Pt(5 MLs)/MnPt (2 u.c.) film around Fermi energy with $E = -0.2$ V/Å and without electric field. One can notice that the DOS of d_{yz}/d_{xz} slightly increase around Fermi energy under electric field $E = -0.2$ V/Å. For M//[1 1 0], there are two pairs of matrix elements of orbital angular momentum operator involved d_{yz}/d_{xz} are nonzero, and that is $\langle d_{xy}|\ L_{[110]}\ |d_{yz}\rangle = \frac{\sqrt{2}}{2}i$ and $\langle d_{xy}|\ L_{[110]}\ |d_{xz}\rangle = -\frac{\sqrt{2}}{2}i$. The increase of d_{yz}/d_{xz} DOS around Fermi energy by applying electric field may contribute to SOC energy E_{soc} for M//[1 1 0] and thus favor the magnetization easy axis along [1 1 0].

So far the discussions on VCMA effect are focusing on the MnPt (MnPd)/Vacuum interface and the magnitude of the electric field is referred to the field at MnPt and MnPd surface. The VCMA effect can be further magnified by using insulating materials with much larger relative dielectric constant. For instance, $SrTiO_3$ (STO) film, which has a very large relative dielectric constant ε_{STO} (around 100–200) and a small lattice mismatch with MnPt or MnPd (< 2.2%), could be a potential candidate [37,38]. In a MnX (X = Pt, Pd)/$SrTiO_3$/NM (nonmagnetic metal) junctions, the relation between the electric fields at MnX film surface E_{MnX} and inside of $SrTiO_3$ barrier E_{STO} should be : $E_{MnX} = \varepsilon_{STO}E_{STO}$. If the magnitude of electric field is 1 V/nm across the $SrTiO_3$ barrier, the electric field at the MnX/STO interface could be as large as 10 V/Å ($\varepsilon_{STO} = 100$). In addition, the investigated electric field E_{MnX} at the MnPd and MnPt film surfaces is between −0.3 V/Å (-3 V/nm) and + 0.3 V/Å(+3 V/nm). If the insulator with dielectric constant ε is used, the electric field across such barrier will be only E_{MnX}/ε, which should be lower than the breakdown voltage of the dielectric insulator. Therefore the magnitude of the electric field investigated in the work is feasible in the experiments.

In general, the total MCA per unit area in an (anti)ferromagnetic film can be written as the sum of two contributions:

$$K = tK_b + K_i \tag{6}$$

where K_b and K_i are the bulk and interface MCA, and t is the film thickness. For VCMA effect, the spin-dependent screening occurs only at the topmost few layers. Therefore, the applied voltage will mainly change the interface MCA, K_i. In the case of Fe/MgO, because the bulk MCA of Fe is negligible (the MCA of bulk bcc Fe is in 1 μeV per atom [39]), the MCA of Fe/MgO is dominated by the interface MCA K_i. However, for MnPt and MnPd films, they have sizable bulk MCA K_b as we show previously, and therefore only small portion of MCA can be modulated by applying electric field. In consequence, generally, the VCMA effect in MnPt and MnPd films should be smaller than that of Fe/MgO interface. So the VCMA effect should only be pronounced in ultrathin MnPt, MnPd and other antiferromagnetic films which possesses relatively large bulk MCA.

In summary, the VCMA effect on MnPt and MnPd thin films have

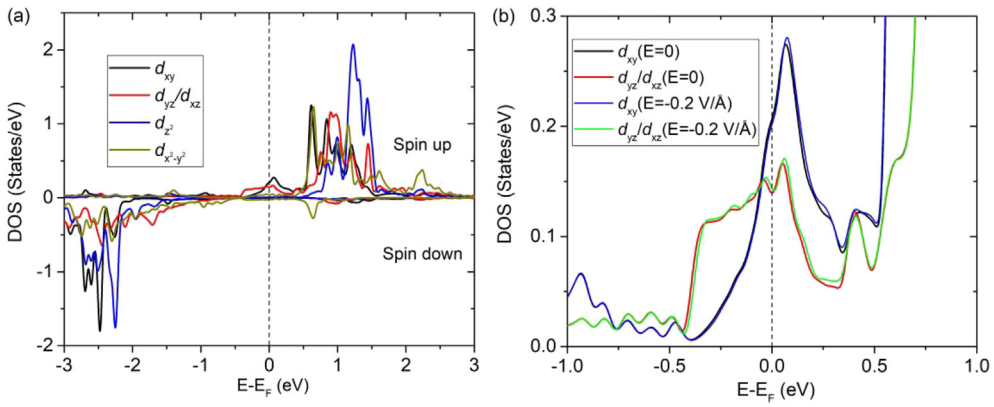

Fig. 5. . (a) The *d*-orbital resolved density of states on surface Mn atom in Pt(5 MLs)/MnPt (2 u.c.) film. (b) The density of states of d_{xy}, d_{yz}/d_{xz} orbitals on surface Mn atom in Pt(5 MLs)/MnPt (2 u.c.) film around Fermi energy under electric field E = -0.2 V/Å and zero electric field E = 0. The vertical dash lines indicate the position of Fermi energy.

been investigated by using first-principles calculations. It is found that both MnPt and MnPd thin films show in-plane magnetic anisotropy and the easy axis could be either along [1 0 0] or [1 1 0] directions depending on the film thickness. We show that the Néel vector of two unit cells of MnPt thin film on Pt(0 0 1) can be switched between [1 0 0] and [1 1 0] in the basal plane by electric field. The VCMA effect in MnPd thin films generally increases linearly with electric field and the magnitudes of the VCMA coefficient for MnPd film is estimated to be around 20 fJ/V/m. The VCMA effect in the studied AFM films can be further enhanced by using $SrTiO_3$ as dielectric materials. Please note that, the switching of Néel vector by applying electric field as we discussed is volatile. For example, for the case of Pt(5 MLs)/MnPt (2 u.c.) film, if the electric field is able to rotate the Néel vector towards [1 1 0] direction, once the electric field has been removed, the Néel vector will restore towards [1 0 0] or [0 1 0] direction randomly. The nonvolatile switching of Néel vector of AFMs may be achieved in AFM/Piezoelectric substrate or AFM/Ferroelectric substrate through the strain or electric polarization effect. That will be the topic of our future investigation. However, similar to the case of VCMA in FMs, the VCMA effect in AFMs investigated here may be used to reduce the energy barrier between different Néel vector directions and lower down the switching current through spin-torque mechanism. Our calculation results suggest that the VCMA effect can potentially be an alternative strategy for the electrical control of the Néel order in antiferromagnetic films and may pave the further experimental and theoretical investigations on the VCMA effect of antiferromagnetic films.

CRediT authorship contribution statement

Yurong Su: Data curation, Writing - original draft, Visualization, Writing - review & editing, Investigation. **Mengyin Li:** Software, Validation. **Jia Zhang:** Conceptualization, Methodology, Writing - review & editing. **Jeongmin Hong:** Investigation. **Long You:** Supervision, Writing - review & editing.

Declaration of Competing Interest

The authors declare that they have no known competing financial interests or personal relationships that could have appeared to influence the work reported in this paper.

Acknowledgement

Long You is supported by the National Natural Science Foundation of China with Grant No. 61674062. Jia Zhang is supported by the National Natural Science Foundation of China with Grant No. 11704135. The calculations in this work are partly performed at National Supercomputer Center in Guangzhou, TianHe-2(B) China.

References

[1] V. Baltz, A. Manchon, M. Tsoi, T. Moriyama, T. Ono, Y. Tserkovnyak, Rev. Mod. Phys. 90 (2018) 015005.
[2] T. Jungwirth, X. Marti, P. Wadley, J. Wunderlich, Nat. Nanotechnol. 11 (2016) 231.
[3] T. Jungwirth, J. Sinova, A. Manchon, X. Marti, J. Wunderlich, C. Felser, Nat. Phys. 14 (2018) 200.
[4] T. Satoh, R. Iida, T. Higuchi, M. Fiebig, T. Shimura, Nat. Photonics 9 (2015) 25.
[5] K. Olejník, T. Seifert, Z. Kašpar, V. Novák, P. Wadley, R.P. Campion, M. Baumgartner, P. Gambardella, P. Němec, J. Wunderlich, J. Sinova, P. Kužel, M. Müller, T. Kampfrath, T. Jungwirth, Sci. Adv. 4 (2018) eaar 3566.
[6] X. Marti, I. Fina, C. Frontera, J. Liu, P. Wadley, Q. He, R.J. Paull, J.D. Clarkson, J. Kudrnovský, I. Turek, J. Kuneš, D. Yi, J.-H. Chu, C.T. Nelson, L. You, E. Arenholz, S. Salahuddin, J. Fontcuberta, T. Jungwirth, R. Ramesh, Nat. Mater. 13 (2014) 367.
[7] P. Wadley, B. Howells, J. Železný, C. Andrews, V. Hills, R.P. Campion, V. Novák, K. Olejník, F. Maccherozzi, S.S. Dhesi, S.Y. Martin, T. Wagner, J. Wunderlich, F. Freimuth, Y. Mokrousov, J. Kuneš, J.S. Chauhan, M.J. Grzybowski, A.W. Rushforth, K.W. Edmonds, B.L. Gallagher, T. Jungwirth, Science 351 (2016) 587.
[8] C. Song, Y. You, X. Chen, X. Zhou, Y. Wang, F. Pan, Nanotechnology 29 (2018) 112001.
[9] L. Liu, C.-F. Pai, Y. Li, H.W. Tseng, D.C. Ralph, R.A. Buhrman, Science 336 (2012) 555.
[10] L. Liu, O.J. Lee, T.J. Gudmundsen, D.C. Ralph, R.A. Buhrman, Phys. Rev. Lett. 109 (2012) 096602.
[11] S. Zhang, Y. Su, X. Li, R. Li, W. Tian, J. Hong, L. You, Appl. Phys. Lett. 114 (2019) 042401.
[12] J. Železný, H. Gao, K. Výborný, J. Zemen, J. Mašek, A. Manchon, J. Wunderlich, J. Sinova, T. Jungwirth, Phys. Rev. Lett. 113 (2014) 157201.
[13] S.Y. Bodnar, L. Šmejkal, I. Turek, T. Jungwirth, O. Gomonay, J. Sinova, A.A. Sapozhnik, H.-J. Elmers, M. Kläui, M. Jourdan, Nat. Commun. 9 (2018) 348.
[14] X.F. Zhou, J. Zhang, F. Li, X.Z. Chen, G.Y. Shi, Y.Z. Tan, Y.D. Gu, M.S. Saleem, H.Q. Wu, F. Pan, C. Song, Phys. Rev. Appl. 9 (2018) 054028.
[15] X.F. Zhou, X.Z. Chen, J. Zhang, F. Li, G.Y. Shi, Y.M. Sun, M.S. Saleem, Y.F. You, F. Pan, C. Song, Phys. Rev. Appl. 11 (2019) 054030.
[16] X. Chen, X. Zhou, R. Cheng, C. Song, J. Zhang, Y. Wu, Y. Ba, H. Li, Y. Sun, Y. You, Y. Zhao, F. Pan, Nat. Mater. 18 (2019) 931.
[17] H. Yan, Z. Feng, S. Shang, X. Wang, Z. Hu, J. Wang, Z. Zhu, H. Wang, Z. Chen, H. Hua, W. Lu, J. Wang, P. Qin, H. Guo, X. Zhou, Z. Leng, Z. Liu, C. Jiang, M. Coey, Z. Liu, Nat. Nanotechnol. 14 (2019) 131.
[18] E.Y. Tsymbal, Nat. Mater. 11 (2012) 12.
[19] J. Zhang, P.V. Lukashev, S.S. Jaswal, E.Y. Tsymbal, Phys. Rev. B 96 (2017) 014435.
[20] J. Zhang, C. Franz, M. Czerner, C. Heiliger, Phys. Rev. B 90 (2014) 184409.
[21] Y. Shiota, T. Nozaki, F. Bonell, S. Murakami, T. Shinjo, Y. Suzuki, Nat. Mater. 11 (2012) 39.
[22] S. Kanai, M. Yamanouchi, S. Ikeda, Y. Nakatani, F. Matsukura, H. Ohno, Appl. Phys. Lett. 101 (2012) 122403.
[23] Y.J. Tang, B.F.P. Roos, T. Mewes, A.R. Frank, M. Rickart, M. Bauer, S.O. Demokritov, B. Hillebrands, X. Zhou, B.Q. Liang, X. Chen, W.S. Zhan, Phys. Rev. B 62 (2000) 8654.
[24] M.F. Toney, M.G. Samant, T. Lin, D. Mauri, Appl. Phys. Lett. 81 (2002) 4565.
[25] I.J. Park, T. Lee, P. Das, B. Debnath, G.P. Carman, R.K. Lake, Appl. Phys. Lett. 114 (2019) 142403.
[26] R.Y. Umetsu, A. Sakuma, K. Fukamichi, Appl. Phys. Lett. 89 (2006) 052504.
[27] J. Neugebauer, M. Scheffler, Phys. Rev. B 46 (1992) 16067.
[28] G. Kresse, D. Joubert, Phys. Rev. B 59 (1999) 1758.
[29] P.E. Blöchl, Phys. Rev. B 50 (1994) 17953.
[30] J.P. Perdew, K. Burke, M. Ernzerhof, Phys. Rev. Lett. 77 (1996) 3865.
[31] J. Wang, A. Gao, W. Chen, X.D. Zhang, B. Zhou, Z. Jiang, J. Magn. Magn. Mater. 333 (2013) 93.
[32] Z. Lu, R.V. Chepulskii, W.H. Butler, Phys. Rev. B 81 (2010) 094437.
[33] A. Lehnert, S. Dennler, P. Błoński, S. Rusponi, M. Etzkorn, G. Moulas, P. Bencok, P. Gambardella, H. Brune, J. Hafner, Phys. Rev. B 82 (2010) 094409.
[34] G.H.O. Daalderop, P.J. Kelly, M.F.H. Schuurmans, Phys. Rev. B 41 (1990) 11919.
[35] H. Hama, R. Motomura, T. Shinozaki, Y. Tsunoda, J. Phys.: Condens. Matter 19 (2007) 176228.
[36] L. Pál, E. Krén, G. Kádár, P. Szabó, T. Tarnóczi, J. Appl. Phys. 39 (1968) 538.
[37] S. Yamamichi, T. Sakuma, K. Takemura, Y. Miyasaka, Jpn. J. Appl. Phys. 30 (1991) 2193.
[38] K. Abe, S. Komatsu, Jpn. J. Appl. Phys. 32 (1993) 4186.
[39] M.D. Stiles, et al., Phys. Rev. B 64 (2001) 104430.